Rigorous Analysis and Network Modeling of the Inset Dielectric Guide

T. ROZZI, SENIOR MEMBER, IEEE, AND STEPHEN J. HEDGES

Abstract—**The inset dielectric guide (IDG) is an easy-to-fabricate alternative to image line and is also less sensitive to loss by radiation at discontinuities. This paper presents a rigorous variational analysis in space domain based on field and network considerations (transverse resonance diffraction). This approach yields an accurate transverse equivalent network for the fundamental mode suitable for evaluation by a desktop calculator. Theoretical and experimental results are in excellent agreement.**

I. INTRODUCTION

CONSIDERABLE EFFORT has been spent on the development of transmission media suitable for microwave and millimeter-wave communications, obvious examples being finline and image line. At high frequencies, as circuit dimensions and tolerances become smaller, the cost of such circuits rises. High circuit costs may in fact become the limiting factor to the every-increasing commercial development in millimeter-wave technology. Thus, the ease of manufacture and capability for mass production are becoming as important as the circuit performance of such media.

Image line is a recognized low-loss transmission media, but its main disadvantage besides manufacturing difficulties is its radiation loss from all practical components. In order to confine the field more to the structure, trapped image guide has been proposed [1], but this is even harder to make, especially for small guide dimensions. In order to overcome such manufacturing difficulties, inset dielectric guide (IDG), shown in cross section in Fig. 1, has been proposed as a low-cost alternative [2]. IDG, which is just a rectangular groove filled with dielectric, has many of the advantages of the trapped image guide without its fabrication problems.

With the high cost of circuit manufacture, the design of circuits using trial and error is prohibitive; to be viable, the transmission media must be accurately characterized to enable circuits to be built that work the first time.

The IDG structure has been analyzed previously, by Zhou and Itoh [3], as an intermediate structure in the analysis of trapped image guide. This analysis used the effective dielectric constant (EDC) method and it gave useful approximate results for the fundamental mode. The singularity imposed on the field by the 90° metal edges, however, causes diffraction, which is important for the accurate evaluation of the modal cutoffs, field distributions, and transmission losses. We will consider here a general solution to the IDG, which yields an accurate equivalent circuit for the fundamental mode.

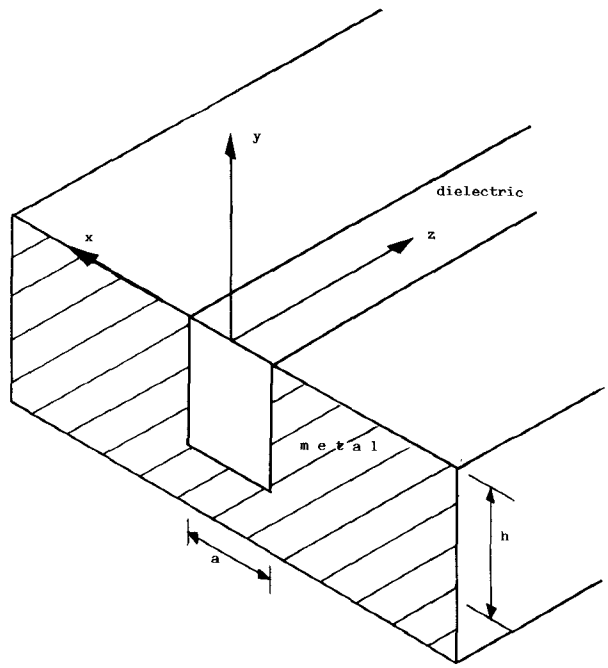

Fig. 1. The cross-sectional structure of inset dielectric waveguide showing the coordinate system used in the analysis.

In recent years, the spectral-domain approach developed by Itoh [4] has been preferred over the space-domain approach for the numerical solution of boundary value problems. In both approaches, the fields are derived from potential functions, which, along with the necessary boundary conditions, can be formulated into sets of integral equations that can be solved for the propagation constant.

In the space-domain approach, these integrals are solved directly by Galerkin's method, the unknown functions being expanded by a suitable set of basis functions. In the spectral-domain approach, the integral equations are transformed into the Fourier domain prior to solution by Galerkin's method. The advantage of the latter method is

Manuscript received December 29, 1986; revised April 23, 1987. This work was supported in part by the S.E.R.C. under Grant GR/C/23407 and Case Award DA 048.

T. Rozzi is with the School of Electrical Engineering, University of Bath, Bath BA2 7AY England.

S. J. Hedges is with the Marconi Research Centre, Great Baddow, Essex, England.

IEEE Log Number 8715667.

that the integral equation is often easier to formulate, the Green's functions often being found by inspection. However, the choice of expansion sets required for solution in the Fourier domain is restricted by the requirement that they have simple Fourier transforms. Thus, functions that do not accurately model the edge conditions are sometimes used, which results in a slow convergence rate.

The approach outlined in this paper is a space-domain approach. Unlike the spectral-domain approach, there is no restriction on the choice of expansion functions. In fact, the functions used are particularly accurate in that they take into account the singularity imposed on the guide field by the 90° metal edges. The problem is formulated so that only one set of basis functions is required, which results in a further increase in accuracy. As a result, the convergence is very rapid, and often only the first term of the expansion set is sufficient.

II. Transverse Resonance Diffraction

The coordinate system used in this analysis is shown, along with the guide structure, in Fig. 1. For each homogeneous region, we may write

$$\epsilon_r k_0^2 = k_x^2 + k_y^2 + \beta^2 \tag{1}$$

where β is the z-directed propagation constant to be determined. For such a composite structure it is easier to solve for propagation in a direction transverse to the homogeneous boundaries, i.e., the y direction.

From the boundary conditions and Maxwell's equations, integral equations for the transverse field components are set up. In order that they can be solved on a computer, they are transformed via Galerkin's technique into scalar equations. In this approach, the integral equations are transformed into the space spanned by the set of functions used to discretize the unknown field components E_x and E_z. These functions are chosen to model as accurately as possible the field components so that few terms are needed for adequate convergence. This includes taking into account the diffraction of the field due to the presence of the 90° metal edges at $x = \pm a/2$, $y = 0$.

The scalar equations so obtained describe propagation in the transverse direction. The resonant frequencies of this equivalent network are those frequencies for which the total admittance at any point in the circuit vanishes. Thus, for a given value of k_0, the propagation constant is found as that value that causes the total transverse admittance to vanish [5]–[8].

This approach is found to give fast convergence for the value of beta. For most practical applications, a 2 by 2 or, at most, a 4 by 4 matrix is all that is required to be solved.

III. Formulation of Admittance Operators

The transverse discontinuity at $y = 0$ in the guide cross section (i.e., the diffraction due to the metal edges) results in a hybrid mode structure. Thus a full six-field analysis is required. The six field components can be obtained from the superposition of z-directed LSE and LSM modes. For propagation in the y direction, these appear to be y-directed TE and TM modes. Thus, the hybrid mode can be derived from y-directed electric and magnetic Hertzian vector potentials, Π_h and Π_e.

These are of the form

$$\Pi_e = \boldsymbol{a}_y \psi_e(x, y) e^{-j\beta z} \qquad \Pi_h = \boldsymbol{a}_y \psi_h(x, y) e^{-j\beta z}. \tag{2}$$

From the potentials, the fields are derived by

$$\boldsymbol{E} = -j\omega\mu_0 \nabla \times \Pi_h + \epsilon r k_0^2 \Pi_e + \nabla\nabla \cdot \Pi_e \tag{3a}$$

$$\boldsymbol{H} = j\omega\epsilon_0\epsilon_r \nabla \times \Pi_e + \epsilon_r k_0^2 \Pi_h + \nabla\nabla \cdot \Pi_h. \tag{3b}$$

The scalars $\psi_e(x, y)$ and $\psi_h(x, y)$ must be chosen to satisfy the correct boundary conditions for the field components and have dimensional consistency. In the following analysis, the z dependence $e^{-j\beta z}$ will be suppressed.

The IDG structure can be considered to be a dielectric-filled rectangular waveguide with one of the side walls removed. Hence, the field in the slot can be constructed from the superposition of discrete waveguide mode functions. In the air region, of course, a continuous spectrum of solutions is possible. The field in each region will thus have to be derived from separate sets of potential functions, which must be continuous across the interface between the two regions.

The admittance operators are formulated from the transverse equivalent circuit. For propagation in the y direction, the slot appears as a short-circuited length of dielectric-filled parallel-plate waveguide radiating into free space. Considering only even-mode solutions with respect to x, then the potential functions are chosen as follows.

In the slot region,

$$\psi_e(x, y) = \sum_{n=0,2\cdots}^{\infty} \frac{I_n'}{j\omega\epsilon} \frac{1}{\left[\left[\frac{n\pi}{a}\right]^2 + \beta^2\right]^{1/2}} \phi_{en}(x) \cdot \frac{\cos k_n (y + h)}{\cos k_n h} \tag{4a}$$

$$\psi_h(x, y) = \sum_{n=0,2\cdots}^{\infty} \frac{V_n''}{j\omega\mu_0} \frac{1}{\left[\left[\frac{n\pi}{a}\right]^2 + \beta^2\right]^{1/2}} \phi_{hn}(x) \cdot \frac{\sin k_n (y + h)}{\sin k_n h} \tag{4b}$$

where

$$\phi_{hn}(x) = \frac{2\delta_n}{\sqrt{a}} \cos\left[\frac{n\pi}{a}\right] x \qquad \phi_{en}(x) = \frac{2}{\sqrt{a}} \sin\left[\frac{n\pi}{a}\right] x$$

$$\delta_n = \frac{1}{\sqrt{2}} \quad n = 0 \qquad \delta_n = 1 \quad n \neq 0$$

and the conservation of wavenumber gives

$$\epsilon_r k_0^2 = k_n^2 + \left[\frac{n\pi}{a}\right]^2 + \beta^2.$$

In the air region,

$$\psi_e(x,y) = \int_0^\infty d\rho \frac{I'(\rho)}{j\omega\epsilon_0} \frac{1}{\sqrt{\rho^2+\beta^2}} \phi_e(x,\rho) e^{-jk_y y} \quad (4c)$$

$$\psi_h(x,y) = \int_0^\infty d\rho \frac{V''(\rho)}{j\omega\mu_0} \frac{1}{\sqrt{\rho^2+\beta^2}} \phi_h(x,\rho) e^{-jk_y y} \quad (4d)$$

where $\phi_h(x,\rho) = \sqrt{2}/\pi \cos \rho x$, $\phi_e(x,\rho) = \sqrt{2}/\pi \sin \rho x$ and the conservation of wavenumber gives

$$k_0^2 = k_y^2 + \rho^2 + \beta^2.$$

The orthogonal sets $\phi_{hn}(x)$ and $\phi_h(x,\rho)$ are normalized so that

$$\int_0^{a/2} \phi_{hn}(x)\phi_{hm}(x)\,dx = \delta_{nm}$$

$$\int_0^\infty \phi_h(x,\rho)\phi_h(x,\rho')\,d\rho = \delta(\rho-\rho'). \quad (5)$$

The amplitude functions are chosen for the sake of convenience and in order to give the unknown amplitudes V_n'' and I_n' the dimensions of a voltage and current, respectively. This will become useful when circuit analogies are made.

By placing the potential functions (4) into (3), the field components in the slot can be found to be

$$E_x = \sum_{n=0,2}^{N} E_{xn}\phi_{hn}(x) \frac{\sin k_n(y+h)}{\sin k_n h} \quad (6a)$$

$$E_y = \sum_{n=2,4}^{N} E_{yn}\phi_{en}(x) \frac{\cos k_n(y+h)}{\cos k_n h} \quad (6b)$$

$$E_z = \sum_{n=2,4}^{N} E_{zn}\phi_{en}(x) \frac{\sin k_n(y+h)}{\sin k_n h} \quad (6c)$$

$$H_x = \sum_{n=2,4}^{N} H_{xn}\phi_{en}(x) \frac{\cos k_n(y+h)}{\cos k_n h} \quad (6d)$$

$$H_y = \sum_{n=0,2}^{N} H_{yn}\phi_{hn}(x) \frac{\sin k_n(y+h)}{\sin k_n h} \quad (6e)$$

$$H_z = \sum_{n=0,2}^{N} H_{zn}\phi_{hn}(x) \frac{\cos k_n(y+h)}{\cos k_n h}. \quad (6f)$$

Analogous expressions can be found for the air region. The amplitudes E_{xn}, E_{yn}, etc., are as yet unknown.

It is desired that the E fields transverse to y in (6) be retained as the unknown quantities, whereas the two remaining quantities transverse to y, i.e., H_z, H_x, be expressed in terms of the above two. By straightforward Fourier analysis of (6) over the slot, it is possible to express each set of amplitudes, e.g., H_{zn}, as a linear operation on the amplitudes E_{xn}, E_{zn}. This linear transformation can be written compactly by means of linear integral operators acting on the fields $E_x(x,0), E(x,0)$ to give the field $H_z(x,0)$, namely

$$\begin{aligned} H_z(x,0) &= \int_0^{a/2} Y_{11}(x,x',y=y'=0)E_x(x',0)\,dx \\ &\quad + \int_0^{a/2} Y_{12}(x,x';y=y'=0)E_z(x',0)\,dx' \\ &\equiv \tilde{Y}_{11}\cdot E_x + \tilde{Y}_{12}\cdot E_z \end{aligned} \quad (7)$$

and similarly for $H_z(x,0)$. Analogous expressions hold in the air region. Thus we obtain for each region integral equations of the type

$$\pm\begin{bmatrix} H_z(x,0) \\ -H_x(x,0) \end{bmatrix} = \begin{bmatrix} \tilde{Y}_{11}^{s,a} & \tilde{Y}_{12}^{s,a} \\ \tilde{Y}_{21}^{s,a} & \tilde{Y}_{22}^{s,a} \end{bmatrix} \cdot \begin{bmatrix} E_x(x,0) \\ E_z(x,0) \end{bmatrix} \quad (8)$$

where the symbols s, a and the signs on the LHS refer to the slot and air region, respectively.

The signs are consistent with power flow into each region from the interface. Continuity of the fields at the interface ($y=0$) will give an integral equation in the unknowns $E_x(x,0), E_z(x,0)$. In order that both unknowns can be expanded in terms of the same set of functions, we require that they display the same x dependence. This will be so if, instead of $E_z(x,0)$, the problem is formulated in terms of $dE_z(x,0)/dx$. As an added bonus, proper convergence of the admittance operators will also result from this transformation. Thus, by integration by parts of (8), we obtain

$$\pm\begin{bmatrix} \pi/a \int_{H_x} H_z\,dx \end{bmatrix} = \begin{bmatrix} \tilde{Y}_{11}^{s,a} & \tilde{Y}_{12}^{s,a} \\ \tilde{Y}_{21}^{s,a} & \tilde{Y}_{22}^{s,a} \end{bmatrix} \cdot \begin{bmatrix} E_x \\ a/\pi\, dE_z/dx \end{bmatrix}. \quad (9)$$

As shown by Itoh [4], a hybrid field can be resolved into pure TE or TM components by a coordinate rotation about the direction of propagation. Following this procedure, angles can be defined that give rise to pure TE ($I_n' = 0$) or TM ($V_n'' = 0$) fields. In the slot region, these angles are defined as

$$\cos\theta = \frac{\frac{n\pi}{a}}{\left[\left(\frac{n\pi}{a}\right)^2+\beta^2\right]^{1/2}} \qquad \sin\theta = \frac{\beta}{\left[\left(\frac{n\pi}{a}\right)^2+\beta^2\right]^{1/2}}$$

and for the air region,

$$\cos\theta = \frac{\rho}{[\rho^2+\beta^2]^{1/2}} \qquad \sin\theta = \frac{\beta}{[\rho^2+\beta^2]^{1/2}}.$$

Using these definitions, the Green admittances obtained from (9) are, in the slot region,

$$Y_{11}^s = \sum_{n=0,2}^{N} \left(Y_n'\cos^2\theta + Y_n''\sin^2\theta\right)\phi_{hn}(x)\phi_{hn}(x') \quad (10a)$$

$$\begin{aligned} Y_{12}^s &= -Y_{21}^s \\ &= \sum_{n=2,4}^{N} j(Y_n' - Y_n'')\cos\theta\sin\theta\left(\frac{1}{n}\right)\phi_{hn}(x)\phi_{hn}(x') \end{aligned} \quad (10b)$$

$$Y_{22}^s = \sum_{n=2,4}^{N} \left(Y_n'\sin^2\theta + Y_n''\cos^2\theta\right)\left(\frac{1}{n}\right)^2 \phi_{hn}(x)\phi_{hn}(x'). \quad (10c)$$

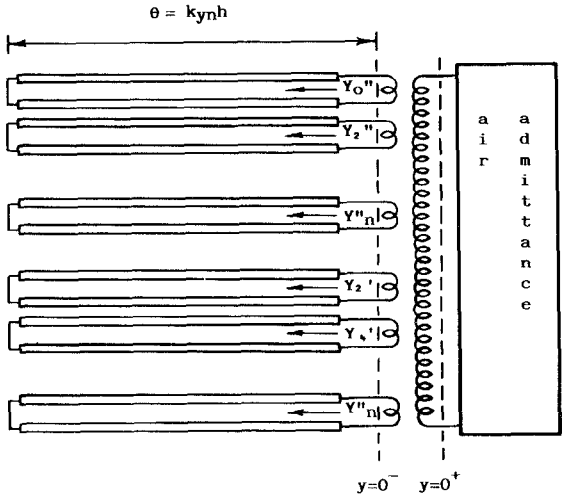

Fig. 2. The transverse equivalent circuit representation for inset dielectric waveguide.

In the air region, the admittances are

$$Y_{11}^a = \int_0^\infty d\rho \left(Y'(\rho)\cos^2\theta + Y''(\rho)\sin^2\theta\right) \cdot \phi_h(x,\rho)\phi_h(x',\rho) \tag{10d}$$

$$Y_{12}^a = -Y_{21}a = \int_0^\infty d\rho\, j(Y'(\rho)+Y''(\rho)) \cdot \sin\theta\cos\theta\left(\frac{\pi}{a\rho}\right)\phi_h(x,\rho)\phi_h(x',\rho) \tag{10e}$$

$$Y_{22}^a = \int_0^\infty d\rho \left(Y'(\rho)\sin^2\theta + Y''(\rho)\cos^2\theta\right) \cdot \left(\frac{\pi}{a\rho}\right)^2 \phi_h(x,\rho)\phi_h(x',\rho) \tag{10f}$$

where Y_n' and Y_n'' are the input admittances of the slot seen by the nth order TM and TE modes, respectively, i.e.,

$$Y_n' = -j\frac{\omega\epsilon}{k_n}\cot(k_n h) \qquad Y_n'' = -j\frac{k_n}{\omega\mu_0}\cot(k_n h).$$

In the air region, $Y'(\rho)$ and $Y''(\rho)$ are the admittances of the TM and TE plane waves:

$$Y'(\rho) = \frac{\omega\epsilon_0}{k_y(\rho)} \qquad Y''(\rho) = \frac{k_y(\rho)}{\omega\mu_0}.$$

This formulation gives rise to the transverse equivalent circuit representation shown in Fig. 2. The slot field is composed of an infinite number of TE and TM components which are transformed (by the coordinate rotation) into a radiation admittance. It is noted that this formulation can easily be modified to take into account changes in the transverse geometry of the structure, as is shown later.

IV. Development of the Dispersion Equation

Bearing in mind that the admittance operators have been defined for each region for power flow into each region from the interface, continuity of the fields at ($y = 0$) gives the equation

$$[\tilde{Y}]\cdot\begin{bmatrix} E_x(x,0) \\ \frac{a}{\pi}dE_z(x,0)/dx \end{bmatrix} = 0 \tag{11}$$

where

$$\tilde{Y} = \tilde{Y}^s + \tilde{Y}^a.$$

For this equation to be solved, it needs to be discretized. The equation is discretized by transforming it into the function space spanned by the set used to expand the unknown $E_x(x,0)$ and $E_z'(x,0)$. The choice of a finite expanding set is crucial in achieving rapid convergence in the dispersion equation; if the choice satisfies the edge condition, then the "scalar products" in (11) will converge rapidly and only a few terms may be needed.

The singularity from a 90° metal edge can be shown to be of the order $r^{-1/3}$ [9]. Thus we seek an orthogonal set of functions that can be weighted by a term that takes into account the effect of the singularity. A function that shows the correct singularity behavior at $x = \pm a/2$ and has a continuous derivative is given by

$$W(x) = \left[1+\left[\frac{2x}{a}\right]\right]^{-1/3}\left[1-\left[\frac{2x}{a}\right]\right]^{-1/3} = \left[1-\left[\frac{2x}{a}\right]^2\right]^{-1/3}. \tag{12}$$

With such a weight function, an obvious choice for the basis terms are the Gegenbauer polynomials $C_m^{1/6}(x)$ [10]. Thus we expand the field unknowns in terms of a weighted set of the normalized even Gegenbauer polynomials (Appendix I):

$$F_m(x) = \frac{1}{N_m}C_m^{1/6}\left[\frac{2x}{a}\right], \qquad m = 0,2,\cdots \tag{13}$$

so that

$$E_x(x,0) = W(x)\sum_{m=0,2\cdots}^{\infty} X_m f_m(x) \tag{13a}$$

$$\left[\frac{a}{\pi}\right]dE_z(x,0)/dx = W(x)\sum_{m=2,4}^{\infty} Z_m f_m(x). \tag{13b}$$

Amplitude plots of the weighted basis terms for $n = 0,2,4,6$ are given in Fig. 3.

Note that, in order to satisfy the boundary conditions of the $E_z(x,0)$ field component, the summation in (13b) contains no constant term and starts from $n = 2$. The coefficients X_n and Z_n are the as yet undetermined amplitudes.

With such a basis set, the mode functions $\phi_{hn}(x)$ and $\phi_h(x,\rho)$ are expanded as

$$\phi_{hn}(x) = \sum_{m=0,2,\cdots}^{\infty} P_{mn} f_m(x)$$

$$\phi_h(x,\rho) = \sum_{m=0,2,\cdots}^{\infty} P_m(\rho) f_m(x) \tag{14}$$

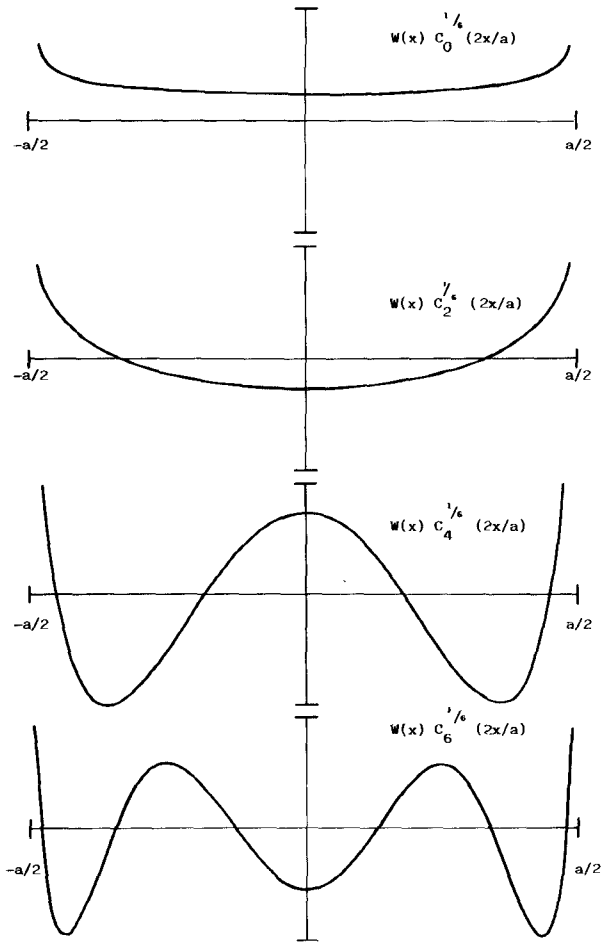

Fig. 3. Amplitude plots of the first four basis terms.

where the inner products P_{mn} and $P_m(\rho)$, evaluated across the half slot, are defined as

$$P_{mn} = \langle W(x) f_m(x) \phi_{hn}(x) \rangle \equiv \int_0^{a/2} W(x) f_m(x) \phi_{hn}(x)\, dx \tag{15}$$

$$P_m(\rho) = \langle W(x) f_m(x) \phi_h(x, \rho) \rangle. \tag{16}$$

The evaluation of P_{mn} and $P_m(\rho)$ is given in Appendix I.

Upon substituting the series expansions for the fields in (11) and carrying out the integration, we obtain the matrix equation

$$[Y] \cdot \begin{bmatrix} X \\ Z \end{bmatrix} = 0. \tag{17}$$

This equation has a nontrivial solution when

$$\det |Y| = 0. \tag{18}$$

In order to recover a scalar transverse equivalent circuit, it is convenient to consider the fundamental transverse propagating mode in the slot, seen as a parallel-plate waveguide terminated by a short circuit at $y = -h$. This is incident upon a discontinuity (the transition between the two regions) and thus excites the radiation modes in the air region and the higher order nonpropagating transverse modes in the slot. In this manner, the fundamental slot mode can be isolated in (11) and all the other contributions lumped together to give

$$[\tilde{Y}] \cdot \begin{bmatrix} E_x(x,0) \\ \frac{a}{\pi} dE_z(x,0)/dx \end{bmatrix} = \begin{bmatrix} -H_{z0}\phi_{h0}(x) \\ 0 \end{bmatrix} \tag{19}$$

where $\tilde{Y} = \tilde{Y}'^s + \tilde{Y}^a$, and $\tilde{Y}'^s$ is the slot admittance operator with fundamental term removed. Also, the quantity $\tilde{Y}$ denotes from now on the total admittance with the fundamental term removed.

Upon discretization (19) becomes

$$[Y] \cdot \begin{bmatrix} X \\ Z \end{bmatrix} = (-H_{z0}) \cdot \begin{bmatrix} P_0 \\ 0 \end{bmatrix}. \tag{20}$$

Rearranging,

$$\begin{bmatrix} X \\ Z \end{bmatrix} = (-H_{z0}) Y^{-1} \cdot \begin{bmatrix} P_0 \\ 0 \end{bmatrix}. \tag{21}$$

Multiply both sides by $[P_0/0]^\tau$:

$$[P_0^\tau, 0^\tau] \begin{bmatrix} X \\ Z \end{bmatrix} = [P_0^\tau, 0^\tau] Y^{-1} \begin{bmatrix} P_0 \\ 0 \end{bmatrix} (-H_{z0}). \tag{22}$$

However, from (6a) and (13a),

$$P_0^\tau \cdot X = E_{x0} \tag{23}$$

and so

$$\frac{-H_{z0}}{E_{x0}} = \left[(P_0^\tau, 0^\tau) \cdot Y^{-1} \cdot \begin{bmatrix} P_0 \\ 0 \end{bmatrix} \right]^{-1}. \tag{24}$$

The normalized admittance of the fundamental slot mode looking from $y = 0$ toward the short circuit is

$$\frac{H_{z0}}{E_{x0}} = -j \cot k_{y0} h. \tag{25}$$

Equation (24) represents the admittance of all the higher order slot modes and air waves as seen from the interface. At resonance the total admittance seen from both sides of the interface must total zero. Therefore the equation for resonance is

$$-j \cot k_{y0} h + \left[[P_n^\tau 0] \cdot \begin{bmatrix} Y_{11} & Y_{12} \\ Y_{21} & Y_{22} \end{bmatrix}^{-1} \cdot \begin{bmatrix} P_0 \\ 0 \end{bmatrix} \right]^{-1} = 0. \tag{26}$$

When N basis terms are used, $\tilde{Y}_{11}$ becomes an N by N matrix, $\tilde{Y}_{12}$ becomes N by $N-1$, $\tilde{Y}_{21}$ becomes $N-1$ by N, and $\tilde{Y}_{22}$ becomes $N-1$ by $N-1$. The overall admittance matrix becomes a square matrix of order $(2N-1)$.

The elements of the admittance matrices of the slot region occurring in (26) can be found from (10a)–(10c) to be

$$(Y_{11}^s)_{km} = -ju \sum_{n=2,4,\cdots}^{\infty} \frac{\coth \sqrt{n^2 - u^2}\,(\pi h/a)}{\sqrt{n^2 - u^2}} P_{kn} P_{mn} \tag{27}$$

and so on, where

$$u \equiv \frac{a}{\pi}\sqrt{\epsilon_r k_0^2 - \beta^2} \qquad k_n = \frac{\pi}{a}\sqrt{u^2 - n^2}$$

$$k = 0,2,4,\cdots \quad m = 0,2,4,\cdots \quad \text{for } Y_{11}$$
$$k = 0,2,4,\cdots \quad m = 2,4,6,\cdots \quad \text{for } Y_{12}$$
$$k = 2,4,6,\cdots \quad m = 0,2,4,\cdots \quad \text{for } Y_{21}$$
$$k = 2,4,6,\cdots \quad m = 2,4,6,\cdots \quad \text{for } Y_{22}.$$

Corresponding expressions are derived from (10d) and (10e) for the admittance matrices of the air region. The apparent pole singularity at $\rho = 0$ in (10e) and (10f) is in fact compensated by a zero of $P_m(\rho)$ there.

V. Analysis of the Partially Filled IDG

In order that the perturbation of the field by the 90° edges may be minimized, it may be feasible to lower the level of the dielectric filling in the slot. Such a change in transverse circuit is easily accommodated by the formulation. For this structure the resonance condition is still enforced by the plane $y = 0$, so that the air admittance operators are unchanged. The admittance operators for the slot region must be modified to take into account the new y variation. The y dependence is given for $\psi_e(x, y)$ and $\psi_h(x, y)$, respectively, as the current and voltage variation along a cascaded section of transmission line. Hence, with suitable normalization, the potentials become

$$\psi_e(x,y) = \sum_{n=0,2}^{\infty} \frac{I'n}{j\omega\epsilon} \frac{1}{\left[\left[\frac{n\pi}{a}\right]^2 + \beta^2\right]^{1/2}} \phi_{en}(x) \left[\frac{jY_0' \sin k_{n2} + (y + h_2) + Y_L' \cos k_{n2}(y + h_2)}{jY_0'' \sin k_{n2}h_2 + Y_L' \cos k_{n2}h_2}\right], \qquad h_2 \leqslant y \leqslant 0 \quad (28a)$$

$$\psi_h(x,y) = \sum_{n=0,2,\cdots}^{\infty} \frac{Vn''}{j\omega\mu_0} \frac{1}{\left[\left[\frac{n\pi}{a}\right]^2 + \beta^2\right]^{1/2}} \phi_{hn}(x) \left[\frac{Y_0'' \cos k_{n2}(y + h_2) + jY_L'' \sin k_{n2}(y + h)}{Y_0'' \cos k_{n2}h_2 + jY_L'' \sin k_{n2}h_2}\right] \quad (28b)$$

where

$$Y_L' = -jY_0' \cot k_{n1}h_1 \qquad Y_L'' = -jY_0'' \cot k_{n1}h_1.$$

The subscripts 1 and 2 refer to propagation in the dielectric- and air-filled regions of the slot, respectively (see Fig. 8). With these potential functions, the analysis is repeated directly as before. The modified admittance operators for the partially filled slow case can be found by inspection from (10) by replacing Y_n' and Y_n'' with the TM and TE admittances for a cascaded section of transmission line, demonstrating the adaptability of this approach.

VI. Simplified Transverse Equivalent Circuit

The hybrid field can, by a rotation in the coordinate system established in [4], be resolved into TE and TM components. This is useful in enabling us to develop an equivalent circuit model for the transverse network. This consists of short-circuited lengths of transmission line, one for each TM and TE slot component, which are transformer-coupled via the coordinate rotation and coupled to a radiation admittance. The transverse equivalent circuit is shown in Fig. 2.

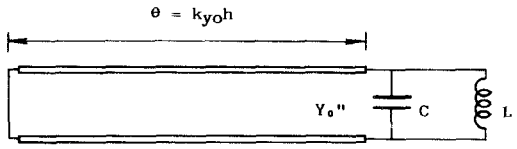

Fig. 4. The simplified transverse equivalent circuit obtained by assuming that only the fundamental slot mode is propagating.

When propagation in the transverse y direction is considered, the admittance terms can be characterized as follows: the Y_{11} and Y_{22} terms give the TE and TM mode admittances, respectively, and the Y_{12} and Y_{21} terms give the coupling between the two polarizations. In general the dispersion equation (26) will contain both TE and TM components. However, when only the first basis term ($m = 0$) is used in (26), the matrix equation reduces to the scalar equation

$$-j\cot\left[\frac{\pi uh}{a}\right] + \frac{Y_{11}}{P_{00}^2} = 0. \quad (29)$$

This equation contains only TE components, thus allowing a simplification to be made to the transverse equivalent circuit. Writing (29) out fully,

$$-j\cot\left[\frac{\pi uh}{a}\right] + ju\sum_{n=2}^{\infty} \frac{\coth\sqrt{n^2 - u^2}\,(\pi h/a)}{\sqrt{n^2 - u^2}} \left[\frac{P_{0n}}{P_{00}}\right]^2 + \frac{w^2}{ju}\int_0^{\infty} d\rho \frac{1}{\sqrt{w^2 - \bar{\rho}^2}} \left[\frac{P_0(\rho)}{P_{00}}\right]^2 = 0 \quad (30)$$

where

$$u = \frac{a}{\pi}\sqrt{\epsilon_r k_0^2 - \beta^2} \qquad w = \frac{a}{\pi}\sqrt{\beta^2 - k_0^2} \qquad \bar{\rho} = \frac{a}{\pi}\rho.$$

This equation contains the "effective" frequency variable u, which is the y-directed wavenumber for the fundamental mode in the slot. Thus, by considering the frequency dependence of (30) with u, the terms can be identified as elements in a transverse equivalent circuit for the fundamental mode. In this way the terms in (30) can be identified as follows: the first term is an inductance in u representing a short-circuited length of transmission line for the fundamental mode. The second term is capacitive and represents the energy storage in the slot due to the

TABLE I
THE VALUES OF PROPAGATION CONSTANT CALCULATED FOR AN X-BAND SAMPLE OF IDG USING THE FIRST THREE ORDERS OF EXPANSION OF THE DISPERSION EQUATION

Frequency (GHz)	First Order ($n=0$)	Second Order ($n=0,2$)	Third Order ($n=0,2,4$)
7	$1.7143 - j0.000185$	$1.7097 - j0.000183$	$1.7095 - j0.000183$
8	$2.0307 - j0.000220$	$2.0258 - j0.000219$	$2.0257 - j0.000219$
9	$2.3464 - j0.000255$	$2.3415 - j0.000254$	$2.3413 - j0.000254$
10	$2.6617 - j0.000289$	$2.6570 - j0.000289$	$2.6568 - j0.000289$
11	$2.9768 - j0.000323$	$2.9722 - j0.000323$	$2.9720 - j0.000323$
12	$3.2914 - j0.000357$	$3.2871 - j0.000356$	$2.2869 - j0.000356$
13	$3.6057 - j0.000390$	$3.6016 - j0.000390$	$3.6015 - j0.000390$

$a = 1.016$ cm; $h = 1.524$ cm; $\epsilon_r = 2.08 - j0.000416$.

nonpropagating modes. The third term describes the energy storage of the nonpropagating TE modes in the air region.

The admittance terms identified in this way give rise to the simple transverse equivalent circuit shown in Fig. 4.

VII. GUIDE LOSS CALCULATIONS

Even in the absence of conduction losses, the solution of the dispersion equation (26) in the complex β plane will give rise to a complex value of β:

$$\beta = \beta' - j\beta''. \tag{31}$$

The complex part of β is due to the losses incurred by radiation away from the guide, and by dissipation in the dielectric.

In a dielectric slab waveguide, radiation loss occurs when β is less than k_0, the cutoff point for a dielectric guide. Physically, this can be seen as the diffraction of the guided wave by the air/dielectric interface, giving rise to a leaky wave in the air region. Above $\beta = k_0$ the guided wave is fully bound in the guide (using the "bouncing ray" analogy, the angle of incidence on the dielectric/air boundary is greater than the critical angle), and so no radiation can occur. In the IDG, the fields peak at the metal corners, as depicted in Fig. 7. In the presence of the slightest irregularity, the propagating mode begins to radiate near cutoff, merging smoothly with a leaky wave below cutoff (see Fig. 11). This effect is not important in the operative range of the guide, and although implicit from the above model, will be omitted in the following calculations.

The dielectric losses can be accounted for by using a complex value for the relative permittivity ϵ_r. The dielectric losses are found to be of the same order as the loss tangent. Table I gives the computed values of β for different orders of expansion of (26). The values were computed for a dielectric filling of PTFE which was assumed to have a loss tangent of 2×10^{-4}.

Calculation of the Conduction Losses

The conduction loss can be found by the classical perturbation approach [5, p. 187]. The corresponding attenuation is given by

$$\alpha_c = \frac{1}{2} \frac{\text{energy dissipated by conducting surfaces}}{\text{energy transmitted along guide}} \quad \text{Np/cm}. \tag{32}$$

This loss, if sufficiently small, will not substantially change the fields in the guide. With this assumption, the loss components can be calculated using the loss-free fields. The field in the guide will induce currents in the conducting walls:

$$\boldsymbol{J}_s = \boldsymbol{n} \times \boldsymbol{H}, \ \boldsymbol{n} = \text{inward directed normal at the guide wall.} \tag{33}$$

These currents will be dissipated as I^2R losses. The surface resistance of a conductor can be expressed as

$$R_m = \sqrt{\frac{\omega \mu_0}{2\sigma}} \tag{34}$$

and so the time-averaged power loss per unit length of guide is given as

$$P_c = \frac{R_m}{2} \int_{\substack{\text{guide} \\ \text{walls}}} J_s \cdot J_s^* dl = \frac{R_m}{2} \int_{\substack{\text{guide} \\ \text{walls}}} (\boldsymbol{n} \times \boldsymbol{H}) \cdot (\boldsymbol{n} \times \boldsymbol{H}^*)\, dl.$$

Due to the guide symmetry, the integrals need only be evaluated over one half of the guide cross section. The currents induced in the ground plane can be neglected, and so

$$P_c = \frac{R_m}{2} \int_0^{a/2} (H_z H_z^* + H_x H_x^*)\, dx + \frac{R_m}{2} \int_{-h}^{0} (H_z H_z^* + H_y H_y^*)\, dy \quad \text{(W/cm)}. \tag{35}$$

The power flow along the guide can be evaluated as the time-averaged Poynting vector over the guide cross section:

$$P = \frac{1}{2} \iint_{\substack{\text{cross} \\ \text{section}}} \text{Re}(\boldsymbol{E} \times \boldsymbol{H}^*) \cdot \boldsymbol{a}_z\, dS \text{(W)}$$

$$\frac{1}{2} \iint_{\substack{\text{cross} \\ \text{section}}} \text{Re}(E_x H_y^* - H_x^* E_y)\, dS. \tag{36}$$

Thus

$$\alpha_c = \frac{P_c}{2P} \quad \text{Np/cm.} \tag{37}$$

Having solved for β, the basis amplitudes $\boldsymbol{X}$ and $\boldsymbol{Z}$ can be found from (21). From these, the mode amplitudes of the field components given in (6) can be found as

$$E_{xn} = \boldsymbol{P}_n^{\tau} \cdot \boldsymbol{X} \tag{38a}$$

$$E_{yn} = -\left[\frac{1}{k_n}\right] \cot k_n h \left[\left[\frac{n\pi}{a}\right] \boldsymbol{P}_n^{\tau} \cdot \boldsymbol{X} + j\beta \left[\frac{1}{n}\right] \boldsymbol{P}_n^{\tau} \cdot \boldsymbol{Z}\right] \tag{38b}$$

$$E_{zn} = \left[\frac{1}{n}\right] \boldsymbol{P}_n^{\tau} \cdot \boldsymbol{Z} \tag{38c}$$

$$H_{xn} = \left[\frac{n\pi}{a}\right] \frac{\cot k_n h}{\omega \mu_0 k_n} \cdot \left[\beta \boldsymbol{P}_n^{\tau} \cdot \boldsymbol{X} + j\left[\frac{a}{\pi}\right]\left[\frac{\epsilon r k_0^2 - \left[\frac{n\pi}{a}\right]^2}{n2}\right] \boldsymbol{P}_n^{\tau} \cdot \boldsymbol{Z}\right] \tag{38d}$$

$$H_{yn} = \frac{1}{j\omega\mu_0}\left[j\beta \boldsymbol{P}_n^{\tau} \cdot \boldsymbol{X} + \left[\frac{\pi}{a}\right] \boldsymbol{P}_n^{\tau} \cdot \boldsymbol{Z}\right] \tag{38e}$$

$$H_{zn} = \frac{1}{\omega\mu_0} \frac{\cot k_n h}{k_n}\left[-jk_{y0}^2 \boldsymbol{P}_n^{\tau} \cdot \boldsymbol{X} + \frac{\pi}{a}\beta \boldsymbol{P}_n^{\tau} \cdot \boldsymbol{Z}\right]. \tag{38f}$$

Similar results can be found for the components in the air region. By substituting these expressions into (6) and evaluating the integrals (35) and (36), the conduction loss can easily be evaluated. For most purposes, it is sufficient to consider the fundamental approximation only so that X_0 is the only finite amplitude term. The expressions (38) are then considerably reduced.

The overall guide loss will be given as

$$\alpha = \alpha_c + \beta''. \tag{39}$$

VIII. Computed and Measured Results

For ease of manufacture and availability of equipment, the experimental prototypes were made from slots 1.016 cm wide, for transition into X-band rectangular waveguide. All measurements were carried out on an HP 8510 analyzer. The substitution measurements were carried out over the X-band (8–12.4 GHz). The dispersion and Q measurements were obtained from iris-coupled resonant lengths of IDG. The irises, being symmetrically placed in the launching guide, did not excite the higher TE_{20} rectangular waveguide mode and so the measurement range was determined by the cutoff of the higher order mode of the IDG. It is noted that the operation band of the IDG is somewhat broader than X-band. The guide dimensions were somewhat arbitrary, although to facilitate the transition to rectangular waveguide the slot width was kept the same as the narrow waveguide dimension. The slot depth again is variable, although for efficient coupling to rectangular waveguide it should be at least one half of the broad waveguide dimension. For the measurements two slot sizes were available, with $h/a = 1.0$ and $h/a = 1.5$. The dielectric inserts were machined from PTFE which had an assumed dielectric constant of 2.08. The transition from rectangular waveguide to IDG was carried out by a dielectric taper, as shown in Fig. 5. The measured SWR of this transition with and without the taper is shown in Fig. 6. The length of the taper in this case was 50 mm and it can be seen that with a taper the SWR of the transition is better than 1:1.12 across the band. It is noted that the length was not optimized; rather, it was arbitrarily chosen so as to be longer than one guided wavelength over the band.

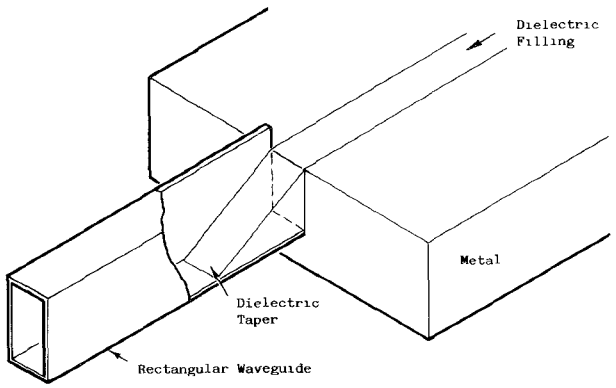

Fig. 5. The transition between rectangular waveguide and IDG.

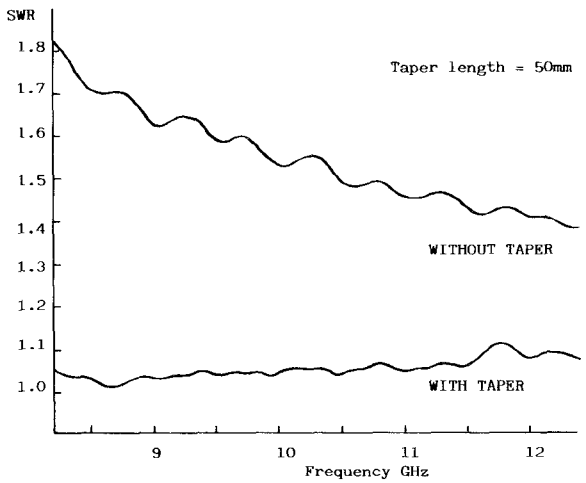

Fig. 6. The measured reflection from a rectangular waveguide to IDG transition with and without a dielectric taper.

The hybrid modes of IDG are designated HE_{nm} or EH_{nm} according to the relative dominance of the TE- or TM-to-y components, respectively. The subscripts n, m refer to the number of half-wave variations across the slot and down the slot. The field magnitude plots of the fundamental HE_{01} mode taken across a transverse section are given in Fig. 7. These were obtained by solving the dispersion equation for β and then using (21) to find the basis amplitude coefficients. These could then be used to calculate the field coefficients in (38), which then gave the fields in (6). The field plots show that the fundamental mode is essentially TE with respect to y with the components E_x, H_y, H_z. In the slot these terms dominate, the TM

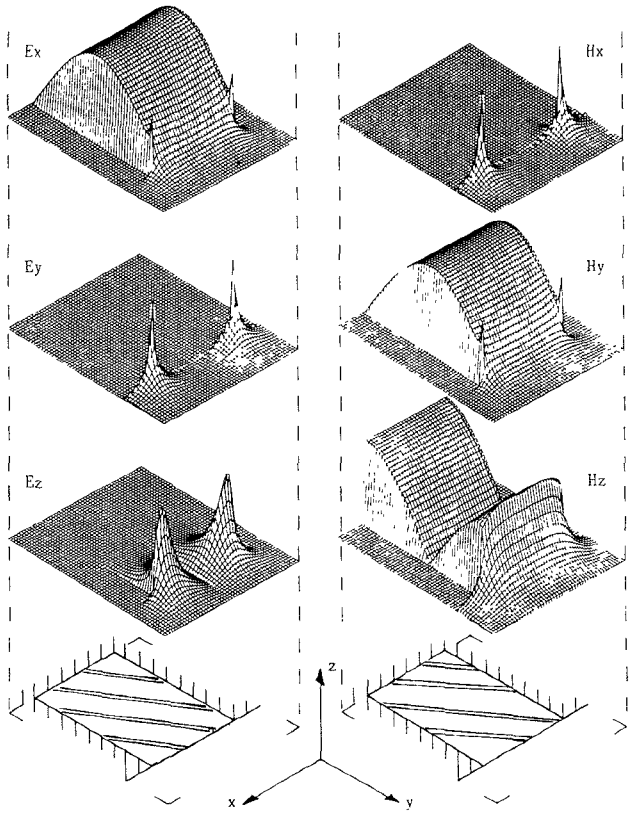

Fig. 7. The field components of the fundamental HE_{01} mode plotted as the magnitude values over the transverse guide section.

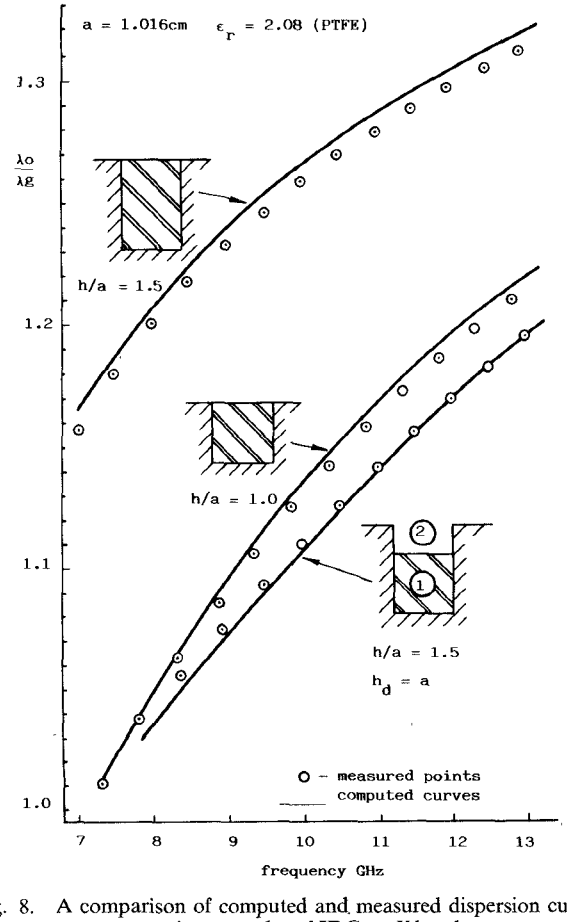

Fig. 8. A comparison of computed and measured dispersion curves for various samples of IDG at X-band.

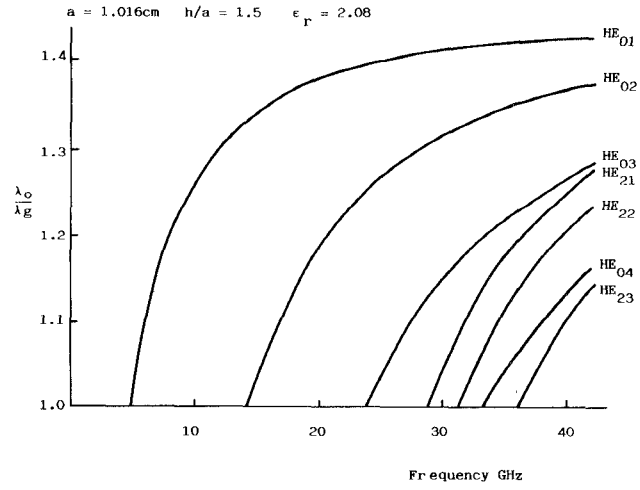

Fig. 9. Computed dispersion curves for the even modes of an X-band sample of IDG up to 40 GHz.

components are only excited in order to satisfy the boundary conditions imposed by the 90° edge. Also evident from the plots is the singularity due to the edge. The z-directed components, as expected, are not affected by the edge and show no singular behavior.

The dispersion characteristics of several IDG geometries were measured by using a resonant line technique. The comparison between the measured and computed results is shown in Fig. 8. The computed results were calculated from a second-order expansion, and are within 1 percent of the measured values. It is noted that the dielectric constant of PTFE was taken to be 2.08, but the uncertainty as to its actual value is ± 2 percent, yielding a ± 1-percent uncertainty in the computed results.

Each term in the basis set models a particular field variation across the slot. For example the $n=2$ term models the modes for which $k_x = (2\pi/a)$. Therefore, when the values of β for the HE_{mn} modes are sought, the expansion must contain at least $m/2$ terms (considering even modes only). In Fig. 9 the dispersion curves for the even modes above cutoff of the X-band IDG are plotted, using the second-order expansions.

The computed loss of a sample of IDG with dimensions 1.016 cm by 1.524 cm and made from copper is given in Table II for two different dielectric fillings. It can be seen that the dielectric loss is of the order of the loss tangent of the dielectric used. Obviously Perspex, with its particularly high loss tangent, would not be used for a practical IDG. The table shows that the large conductor area surrounding the dielectric does not substantially add to the guide loss, while the greater confinement of the field into the dielectric, causing more dielectric loss, does.

The loss of a 20-cm section of IDG made of brass and with PTFE filling was measured using a substitution technique. The comparison with computed values is shown in Fig. 10. The resistivity of the brass was taken to be 6.2×10^{-8} $\Omega\cdot$m and no factor was introduced to take into account any surface roughness. The Q factor of a resonant section of IDG was measured and the results are compared in Fig. 11 with those obtained from the approximate

TABLE II
COMPUTED VALUES OF LOSS FOR A SECTION OF IDG MADE OF COPPER WITH DIMENSIONS 1.016 CM × 1.524 CM

Dielectric Filling of PTFE ($\epsilon_r = 2.08 - j0.000416$)					
Frequency	Conductor Loss	Dielectric and Radiation Loss	Total Loss		Q factor
(GHz)	(Np/cm)	(Np/cm)	dB/wave	dB/m	
8	−0.000103	−0.000220	−0.00870	−0 281	3084.5
9	−0.000110	−0.000255	−0.00850	−0.317	2992.3
10	−0.000117	−0.000289	−0.00833	−0.353	2929.4
11	−0.000123	−0.000323	−0.00818	−0.387	2886.8
12	−0.000128	−0.000357	−0.00804	−0.421	2858 6
Dielectric Filling of PERSPEX ($\epsilon_r = 2.50 - j0.02075$)					
Frequency	Conductor Loss	Dielectric and Radiation Loss	Total Loss		Q factor
(GHz)	(Np/cm)	(Np/cm)	dB/wave	dB/m	
8	−0.000117	−0.0107	−0.2618	−9.37	91.5
9	−0.000124	−0.0122	−0 2591	−10.72	87.7
10	−0.000131	−0.0137	−0.2567	−12.04	85.0
11	−0.000136	−0.0152	−0.2545	−13.34	83.0
12	−0.000141	−0.0167	−0.2524	−14.62	81.6

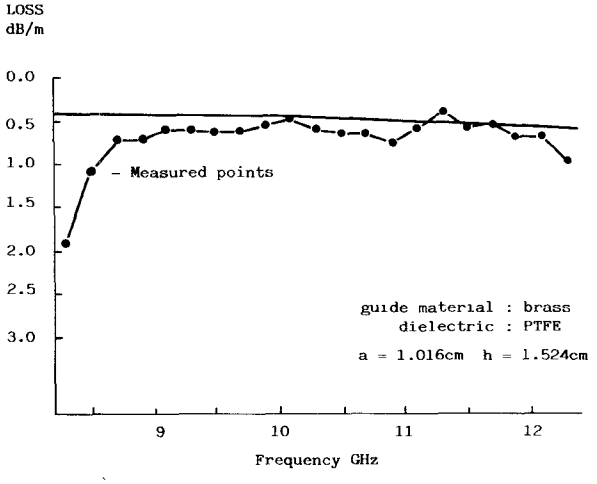

Fig. 10. A comparison of the measured and computed values of loss for a 20-cm section of IDG.

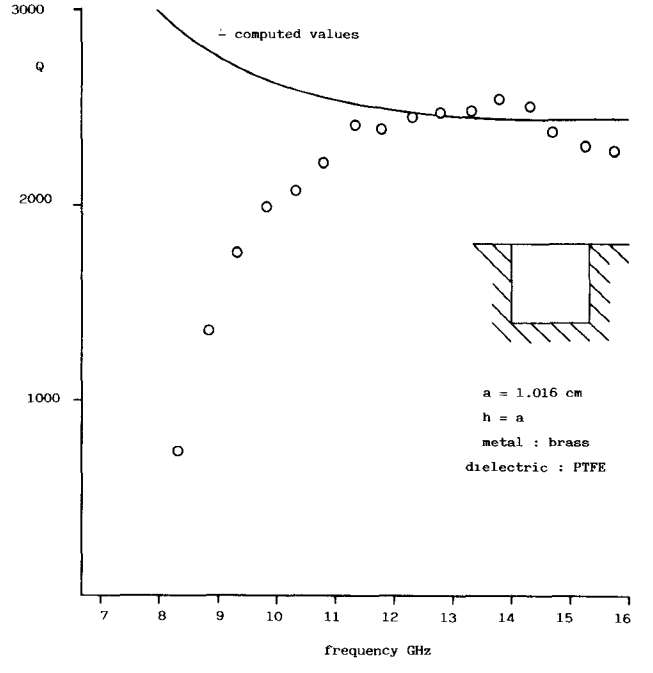

Fig. 11. A comparison between the measured and computed Q values of a resonant section of IDG.

formula derived in Appendix II. It can be seen from both figures that there is a discrepancy between the computed and measured results at the lower frequencies. This is due to the fact that radiation loss mainly due to edge diffraction has not been taken into account. This loss will be more pronounced at lower frequencies. The analysis has shown a good correlation with the measured results. However it is noted that the samples measured approached the ideal structure in that the dielectric was machined to closely fit the slot. Practical structures for high mm wave use will be constructed from casting resins or screen printing [11] and so will depart more from the ideal structure.

Investigation into the increased loss due to air voids at the metal/dielectric boundaries and dielectric inhomogeneities are not considered here but merit further attention.

IX. Conclusions

This work describes a highly accurate method for the analysis of IDG with a minimum of computational effort. The method can be easily adapted to such structures as ridged waveguide and finline with thick conductors.

The propagation constants of the first few modes and the loss of IDG have been calculated, showing good agreement with measured results. It has been shown that, in the practical operating range, the loss is dominated by the dielectric loss.

Appendix I
The Determination of the Coefficients P_{mn} and $P_m(\rho)$

The coefficients P_{mn} and $P_m(\rho)$ have been defined as

$$P_{nm} = \langle W(x) f_m(x) \phi_{hn}(x) \rangle \tag{A1}$$

$$P_m(\rho) = \langle W(x) f_m(x) \phi_h(x, \rho) \rangle \tag{A2}$$

where

$$\phi_{hn}(x) = \frac{2\delta_n}{\sqrt{a}} \cos(n\pi/a)x \qquad \phi_h(x, \rho) = \sqrt{\frac{2}{\pi}} \cos \rho x \tag{A3}$$

and the weighting function, defined to model the edge singularity, is

$$W(x) = \left(1-(2x/a)^2\right)^{-1/3}. \tag{A4}$$

From tables [10] the integral is found:

$$\int_0^1 (1-t^2)^{v-1/2} C_{2n}^v(t)\cos bt\,dt = \frac{(-1)^n \pi \Gamma(2n+2v) J_{v+2n}(b)}{(2n)!\Gamma(v)(2b)^v} \qquad [\mathrm{Re}\, v > -1/2, b > 0]. \tag{A5}$$

With the substitutions $v=1/6$, $t=2x/a$, $b=n\pi/2$, and $m=2n$, we can write

$$P_{mn} = \frac{1}{N_m} \frac{\delta_n \sqrt{a}\,(-1)^{m/2}\pi\Gamma\left[m+\frac{1}{3}\right] J_{m+1/6}\left[\frac{n\pi}{2}\right]}{m!\Gamma\left[\frac{1}{6}\right](n\pi)^{1/6}} \tag{A6}$$

where

$$N_m^2 = \frac{a\pi 2^{-4/3}\Gamma\left[m+\frac{1}{3}\right]}{m!\left[m+\frac{1}{6}\right]\left[\Gamma\left[\frac{1}{6}\right]\right]^2}. \tag{A7}$$

These expressions are valid only for $n>0$. Taking the limit of (A6) as $n\to 0$ gives

$$P_{00} = \frac{1}{N_0} \frac{\sqrt{a}\,\pi\Gamma\left[\frac{1}{3}\right]}{\Gamma\left[\frac{1}{6}\right]2^{5/6}\Gamma\left[1+\frac{1}{6}\right]} \tag{A8}$$

$$P_{m0} = 0. \tag{A9}$$

Similar expressions hold for $P_m(\rho)$, with the substitution

$$P_m(\rho) = \sqrt{\frac{a}{2\pi}}\, P_{m\bar{\rho}} \qquad \bar{\rho} = \frac{a}{\rho}\rho \tag{A10}$$

Equation (A6) is in fact valid for real $n=\bar{\rho}$.

Appendix II
Approximate Evaluation of the Q Factor

Assuming monomode operation only, the Q factor can be defined as

$$Q = \frac{\omega\langle W\rangle}{\langle Pd\rangle} \tag{A11}$$

where $\langle W\rangle$ is the time-averaged total energy stored in the propagating mode per unit length (J/cm), and $\langle Pd\rangle$ is the time-averaged power lost from propagating mode per unit length (W/cm). If $\langle Pf\rangle$ is the time-averaged power flow along guide, then

$$\alpha = \frac{1}{2}\frac{\langle Pd\rangle}{\langle Pf\rangle}$$

and so

$$Q = \frac{1}{2\alpha}\frac{\omega\langle W\rangle}{\langle Pf\rangle}. \tag{A12}$$

However, the group velocity is

$$\frac{\langle Pf\rangle}{\langle W\rangle} = \frac{\lambda_0}{\lambda g}\frac{c}{\sqrt{\epsilon_r}}.$$

Therefore,

$$Q = \frac{1}{2\alpha}\frac{\omega\lambda g\sqrt{\epsilon_r}}{\lambda_0 c} = \frac{\sqrt{\epsilon_r}K_0^2}{\sqrt{2}\,\alpha\beta}. \tag{A13}$$

Acknowledgment

The authors would like to thank Mr. S. C. Gratze of Marconi Research Laboratories for his support in this work.

References

[1] T. Itoh and B. Adelseck, "Trapped image guide for millimeter wave circuits," *IEEE Trans. Microwave Theory Tech.*, vol. MTT-28, pp. 1433–1436, Dec. 1980.
[2] S. C. Gratze, "Inset dielectric waveguides, Proposal YB0 881," Marconi Research Labs.
[3] W. Zhou and T. Itoh, "Analysis of trapped image guides using effective dielectric constant and surface impedances," *IEEE Trans. Microwave Theory Tech.*, vol. MTT-30, pp. 2163–2166, Dec. 1982.
[4] T. Itoh, "Spectral domain immittance approach for dispersion characteristics of generalised printed transmission lines," *IEEE Trans. Microwave Theory Tech.*, vol. MTT-28, pp. 733–736, July 1980.
[5] S. T. Peng and A. A. Oliner, "Guidance and leakage properties of a class of open dielectric waveguides," Part 1, *IEEE Trans. Microwave Theory Tech.*, vol. MTT-29, pp. 843–855, Sept. 1981.
[6] J. Kot and T. Rozzi, "Rigorous modelling of single and coupled rectangular dielectric waveguides by transverse resonance diffraction," in *Proc. 14th European Microwave Conf.* (Liege), Sept. 1984, pp. 424–429.
[7] N. Dagli and C. G. Fonstad, "Analysis of rib dielectric waveguides," *IEEE J. Quantum Electron.*, vol. QE-21, pp. 315–321, Apr. 1985.
[8] M. Koshiba and M. Suzuki, "Vectorial wave analysis of dielectric waveguides for optical-integrated circuits using equivalent network approach," *IEEE J. Lightwave Technol.*, vol. LT-4, pp. 656–664, June 1986.
[9] R. E. Collin, *Field Theory of Guided Waves*. New York: McGraw-Hill, 1960, p. 18.
[10] I. S. Gradshteyn and I. M. Ryshik, *Table of Integrals, Series and Products*. New York: Academic Press, 1965, p. 827.
[11] R. V. Gelsthorpe *et al.*, "Dielectric waveguide: A low-cost technology for millimetre wave integrated circuits," *Radio Electron. Eng.*, vol. 52, nos. 11/12, pp. 552–528, Nov./Dec. 1982.

T. Rozzi (M'76–SM'74) obtained the degree of Dottore in physics from the University of Pisa in 1965 and the Ph.D. degree in electronic engineering at Leeds University in 1968. In 1987 he was awarded the D.Sc. degree by the University of Bath.

From 1968 to 1978 he was a Research Scientist at the Philips Research Laboratories, Eindhoven, the Netherlands, having spent one year (1975) at the Antenna Laboratory, University of Illinois, Urbana. In 1975 he was awarded the Microwave

Prize of the Microwave Theory and Techniques Society of the Institute of Electrical and Electronic Engineers. In 1978 Dr. Rozzi was appointed to the Chair of Electrical Engineering at the University of Liverpool and subsequently appointed to the Chair of Electronics and Head of the Electronics Group at the University of Bath in 1981. From 1983 to 1986 he held the additional responsibility of Head of the School of Electrical Engineering at Bath. Since 1986 Professor Rozzi has also held the "Ordinary Chair" of Antennas at the Faculty of Engineering, University of Ancona, Italy.

Stephen J. Hedges was born in Swindon, U.K., in 1961. He was educated at Bath University, where he obtained the B.Sc. (Hons) degree in electrical engineering in 1983 and the Ph.D. degree in 1987. His research topic was "Inset Dielectric Waveguides."

He joined the Marconi Research Centre, Great Baddow, Essex, in 1987, where he is currently engaged in the investigation of *E*-plane structures and dielectric guides for use in the high microwave range.

Dr. Hedges is a member of the IEE (U.K.).